© 2020. Published by The Company of Biologists Ltd | Development (2020) 147, dev192849. doi:10.1242/dev.192849

RESEARCH ARTICLE

Fgf8 genetic labeling reveals the early specification of vestibular hair cell type in mouse utricle

Evan M. Ratzan[1,2], Anne M. Moon[3,4] and Michael R. Deans[1,5,*]

ABSTRACT

FGF8 signaling plays diverse roles in inner ear development, acting at multiple stages from otic placode induction to cellular differentiation in the organ of Corti. As a secreted morphogen with diverse functions, *Fgf8* expression is likely to be spatially restricted and temporally dynamic throughout inner ear development. We evaluated these characteristics using genetic labeling mediated by *Fgf8*^{mcm} gene-targeted mice and determined that *Fgf8* expression is a specific and early marker of Type-I vestibular hair cell identity. *Fgf8*^{mcm} expression initiates at E11.5 in the future striolar region of the utricle, labeling hair cells following EdU birthdating, and demonstrates that sub-type identity is determined shortly after terminal mitosis. This early fate specification is not apparent using markers or morphological criteria that are not present before birth in the mouse. Although analyses of *Fgf8* conditional knockout mice did not reveal developmental phenotypes, the restricted pattern of *Fgf8* expression suggests that functionally redundant FGF ligands may contribute to vestibular hair cell differentiation and supports a developmental model in which Type-I and Type-II hair cells develop in parallel rather than from an intermediate precursor.

KEY WORDS: FGF8, Hair cell, Vestibular, Inner ear, Cre recombinase, Mouse

INTRODUCTION

The vestibular sensory organs of the vertebrate inner ear contain mechanosensory receptors called hair cells that enable the detection of linear and rotational accelerations of the head, and gravity. Vestibular hair cells can be broadly divided into two classes based upon morphological and synaptic criteria. Type-I hair cells have a characteristic ampoule-like morphology and an afferent nerve terminal which forms a large calyx surrounding the hair cell. In contrast, Type-II hair cells have a columnar morphology and afferent nerve terminals that resemble synaptic boutons. Type-I hair cells are also physiologically unique, with low-voltage activated K^+ currents that enable faster receptor potentials with smaller voltage responses than Type-II hair cells (Rennie et al., 1996; Rusch et al., 1998; Eatock and Songer, 2011).

In the mouse, the terminal mitosis and differentiation of vestibular hair cells begins at embryonic day (E) 11.5 and continues through postnatal development, with over half of the hair cells emerging after birth (Burns et al., 2012; Raft et al., 2007; Ruben, 1967). It has been proposed that hair cells appear sequentially, with the majority of Type-I hair cells developing at embryonic stages and Type-II hair cells emerging postnatally (McInturff et al., 2018). A noteworthy difference between these cell types is the requirement for postnatal expression of *Sox2* in Type-II hair cells, as revealed by the increased number of Type-I hair cells that appear at the expense of the Type-II population after postnatal deletion of *Sox2* (Lu et al., 2019). This has led to the alternative hypothesis that cell identity is determined by Sox2 and is not established until postnatal development, concurrent with Sox2 downregulation in the Type-I cells (Warchol et al., 2019; Hume et al., 2007; Oesterle et al., 2008). The commonalities and differences between these alternative etiologies have been difficult to resolve because the molecular, morphological and synaptic characteristics that distinguish hair cell subtypes are also not available until later postnatal stages [postnatal day (P) 2-12] (Simmons et al., 2010; Perry et al., 2003; McInturff et al., 2018).

Fibroblast growth factor 8 (FGF8) belongs to a family of secreted morphogens that signal locally to neighboring cells to promote differentiation. For example, in the organ of Corti, FGF8 released from inner hair cells induces neighboring pillar cell differentiation. Fewer inner pillar cells differentiate in *Fgf8* knockouts, whereas overexpression leads to ectopic pillar cell formation (Jacques et al., 2007). FGF8 binds with varying specificity and affinity to FGF receptor tyrosine kinases (FGFR1-3) activating intracellular signaling cascades leading to transcription factor activation (Ornitz et al., 1996; Pirvola et al., 2000; Roehl and Nusslein-Volhard, 2001; Firnberg and Neubuser, 2002). Outside of the ear, *Fgf8* is expressed in multiple important signaling centers during embryogenesis and the complete loss of FGF8 function causes early embryonic lethality by disrupting movements of nascent mesoderm in the primitive streak (Crossley and Martin, 1995; Meyers et al., 1998; Sun et al., 1999; Moon and Capecchi, 2000). Studies using hypomorphic *Fgf8* alleles and Cre/Lox-mediated conditional mutagenesis have elucidated crucial roles for FGF8 in left-right axis determination, formation and patterning of the forebrain, olfactory bulb and the cerebellum/midbrain-hindbrain junction, pharyngeal gland development, cardiovascular and craniofacial development, renal development, and limb outgrowth and patterning (Frank et al., 2002; Boulet et al., 2004; Macatee et al., 2003; Reifers et al., 1998; Wright and Mansour, 2003; Lee et al., 1997; Crespo-Enriquez et al., 2012; Griffin et al., 2013; Gao et al., 2018; Lewandoski et al., 2000; Moon and Capecchi, 2000). In the developing neocortex a mutually opposing balance between FGF8 and Emx2 and related transcription factors contributes to functional domain patterning in a process called arealization (Fukuchi-Shimogori and Grove, 2001; O'Leary and Nakagawa, 2002; Muzio and Mallamaci, 2003). Thus, FGF8 can regulate tissue patterning by

[1]Department of Neurobiology and Anatomy, University of Utah School of Medicine, Salt Lake City, UT 84112, USA. [2]Interdepartmental Program in Neuroscience, University of Utah School of Medicine, Salt Lake City, UT 84112, USA. [3]Departments of Molecular and Functional Genomics and Pediatrics, Weis Center for Research, Geisinger Clinic and Geisinger Commonwealth School of Medicine, Danville, PA 17822, USA. [4]Departments of Pediatrics and Human Genetics, University of Utah, Salt Lake City, UT 84112 USA. [5]Department of Surgery, Division of Otolaryngology, University of Utah School of Medicine, Salt Lake City, UT 84132, USA.

*Author for correspondence (michael.deans@utah.edu)

M.R.D., 0000-0001-6319-7945

Handling Editor: François Guillemot
Received 12 May 2020; Accepted 7 October 2020

Development (2020) 147, dev192849. doi:10.1242/dev.192849

signaling between neighboring domains in addition to neighboring cells and is generally necessary for multiple differentiation and patterning events throughout embryonic development.

The diverse roles of FGF8 likely mean that *Fgf8* expression is spatially restricted at different stages of otic development and also highly dynamic as development progresses from one stage to the next. To evaluate this, we examined the spatial and temporal dynamics of *Fgf8* expression during inner ear development using Cre-mediated genetic labeling and *in situ* hybridization (ISH). These analyses were directed towards the vestibular maculae because domains of *Emx2* expression in the utricle and saccule determine hair cell stereociliary bundle orientation (Holley et al., 2010; Jiang et al., 2017) and the reciprocal relationship between FGF8 and Emx2 determines a boundary of *Emx2* expression in the neocortex (Fukuchi-Shimogori and Grove, 2003; Fukuchi-Shimogori and Grove, 2001). We found transient *Fgf8* expression in auditory and vestibular neurons, and sustained specific expression in Type-I hair cells beginning shortly after terminal mitosis at E11.5 and continuing through postnatal development. Genetically labeled vestibular hair cells were distributed throughout the sensory epithelia, exhibited ampoule-like morphology, calyceal afferents, and expressed the molecular marker osteopontin (OPN, also known as Spp1), all of which are consistent with the Type-I hair cell identity. Despite this unique pattern of expression, *Fgf8* conditional knockout mice showed no changes in hair cell types, stereociliary bundle polarity and organization, or formation of the calyx-synapse, suggesting that, as observed in other developmental contexts, there may be functional redundancy with other FGF family members during hair cell development. Although the contribution of FGF signaling to vestibular development remains unknown, genetic labeling experiments demonstrate that hair cell sub-type specification occurs earlier than anticipated, happening shortly after terminal mitosis, and establish *Fgf8* expression as the earliest marker distinguishing vestibular hair cell types.

RESULTS

Generation of the Fgf8^{mcm} allele

Genetic labeling enables heterochronic gene expression studies in which the cells or progeny of cells expressing a gene of interest during a defined period of development can be permanently labeled for evaluation at later stages. To generate a mouse line in which patterns of *Fgf8* gene expression could be evaluated using this approach, cDNA encoding a fusion protein of Cre recombinase flanked by mutated hormone-binding domains of the murine estrogen receptor (mER:Cre:mER) (Verrou et al., 1999) was inserted into the *Fgf8* locus. Commonly called CreER, these modified recombinases localize to the cytoplasm and remain inactive until binding the estrogen analog tamoxifen. Once activated, CreER translocates to the nucleus and catalyzes genetic recombination and excision of DNA located between tandem pairs of 32 base pair LoxP sequences (Zhang et al., 1996). To obtain CreER production in *Fgf8*-expressing tissues without disrupting *Fgf8* function, a cassette containing an IRES sequence (Kaminski et al., 1990; Jang and Wimmer, 1990) followed by the mER:Cre:mER cDNA (Verrou et al., 1999) was inserted into the 3′ untranslated region (UTR) of the *Fgf8* gene (Fig. 1A). This cassette and strategy have been successfully applied at other loci, and Flp-recombinase/Frt-mediated excision of the *NeoR* negative selection gene was completed to avoid hypomorphic effects of *NeoR* on expression from *Fgf8* or other loci (Frank et al., 2002). To determine whether this novel *Fgf8*^{mcm} allele retained intact *Fgf8* expression, phenotypes were examined and *Fgf8* mRNA expression was evaluated in animals heterozygous or homozygous for *Fgf8*^{mcm}.

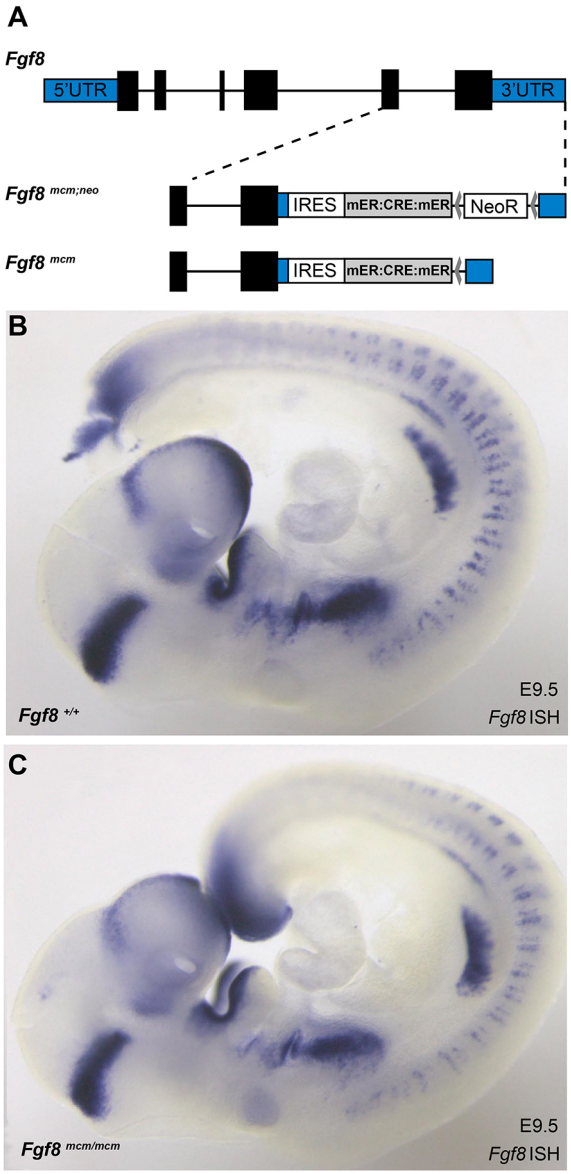

Fig. 1. *Fgf8*^{mcm} engineering strategy does not impact gene expression or function. (A) The gene targeting strategy used to generate *Fgf8*^{mcm} mice inserts an IRES mER:CRE:mER expression cassette into the 3′UTR of the *Fgf8* gene. 5′ and 3′ UTRs are marked in blue shading and the *Fgf8* coding sequence exons are black. An Frt-flanked Neomycin resistance gene (*NeoR*) used for selection of targeted embryonic stem cell clones was removed using FLP recombinase to produce the final *Fgf8*^{mcm} allele. (B,C) Whole-mount ISH for *Fgf8* reveals no detectable differences in the staining pattern or intensity between wild-type (B) and *Fgf8*$^{mcm/mcm}$ homozygous (C) embryos at E9.5.

Whole-mount ISH for *Fgf8* mRNA revealed no detectable difference in hybridization patterns or intensity between wild-type and *Fgf8*$^{mcm/mcm}$ homozygous embryos (Fig. 1B,C). Furthermore, these embryos develop normally without phenotypes observed in *Fgf8* null, hypomorphic or conditional mutant embryos. *Fgf8*$^{mcm/mcm}$ homozygotes survive to adulthood, are indistinguishable from wild-type animals, and reproduce normally. As even a modest decrease in *Fgf8* function has phenotypic consequences in many systems, these results indicate that the presence of the *IRES:mER:Cre:mER* insertion into the 3′ UTR of *Fgf8* does not significantly affect gene function.

Development (2020) 147, dev192849. doi:10.1242/dev.192849

Embryonic Fgf8^{mcm} genetic labeling labels a subset of vestibular hair cells

To evaluate *Fgf8* expression in the developing vestibular system, *Fgf8*$^{mcm/+}$ males were crossed with ROSA$^{ai9tom/ai9tom}$ female mice allowing for tamoxifen-dependent Cre-mediated labeling of *Fgf8*-expressing cells by the red fluorescent protein tdTomato. Single injections of tamoxifen at E17.5 resulted in robust tdTomato expression in a subset of vestibular hair cells identified by βII-spectrin labeling (Fig. 2A-E). Following injections, labeled hair cells were present at E18.5 throughout the utricle (Fig. 2A,B), saccule (Fig. 2C,D) and within the semi-circular canal cristae (Fig. 2E). For each sensory organ, *Fgf8*^{mcm} activation only labeled a subset of the total vestibular hair cells. This readout of *Fgf8* expression is accurate and is unlikely the result of incomplete recombination because it resembles the distribution of *Fgf8* mRNA visualized by whole-mount ISH at P0. *Fgf8* mRNA also appears in a salt-and-pepper pattern within subsets of cells in the utricle (Fig. 2F), saccule (Fig. 2G) and cristae (Fig. 2H). In the cochlea, *Fgf8* mRNA is also present in a subset of hair cells, the single row of inner hair cells, as previously described (Fig. 2I; Jacques et al., 2007).

Interestingly, early injections of tamoxifen at E11.5 similarly labeled a subset of vestibular hair cells when evaluated in the E18.5 utricular maculae (Fig. 3A,B). Previous birthdating experiments using tritiated thymidine or 5-ethynyl-2-deoxyuridine (EdU) incorporation demonstrate that the earliest-born vestibular hair cells undergo terminal mitosis at E11.5 (Ruben, 1967; Jiang et al., 2017) and these cells are enriched in the striolar region of the mature utricle. Similarly, *Fgf8*^{mcm} genetic labeling at E11.5 included striolar hair cells based upon their oncomodulin expression when imaged at E18.5 (Fig. 3A,B) (Simmons et al., 2010; Hoffman et al., 2018). In contrast, induction at later stages (E15.5-E17.5) labeled a broader regional population that included extrastriolar hair cells in the lateral and medial regions (Fig. 2A; Fig. S1). Furthermore, newly-born hair cells labeled by EdU at E12.5 are also genetically labeled by *Fgf8*^{mcm} when EdU and tamoxifen are co-administered (Fig. 3C-E′) and these cells populate the striolar region at E18.5 (Fig. 3C). As EdU is only retained in cells that have undergone their last mitosis, and CreER activation by tamoxifen is transient, colocalization indicates *Fgf8* promoter activation shortly after cell division. Together, these regional and temporal patterns of *Fgf8*^{mcm} activity demonstrate that *Fgf8* expression is initiated in newly-born hair cells, after their specification and during the initial stages of their differentiation, and that expression is maintained throughout embryonic development.

Genetic labeling reveals transient Fgf8 expression in auditory and vestibular neurons

Although tamoxifen injections before E10.5 failed to label hair cells, transient *Fgf8* expression was evident in the spiral ganglion neurons (SGNs) during these early stages of cochlear development. This transient expression follows a development gradient, with tamoxifen injections from E10.5 to E13.5 revealing progressive *Fgf8* activity in SGNs from the cochlear base to the apex (Fig. 4A-C), similar to the expression pattern of pro-neural genes such as neurogenin 1 (Koundakjian et al., 2007). Close examination of the peripheral processes of labeled SGNs show that *Fgf8* is expressed by both Type-I and Type-II SGNs based upon the morphology of tdTomato-labeled peripheral axons innervating the organ of Corti (Fig. 4F). Consistent with previous reports (Jacques et al., 2007), *Fgf8*^{mcm} genetic labeling also robustly marks inner hair cells, with the onset of tdTomato expression also appearing in a developmental gradient initiating in the cochlear base and progressing towards the cochlear apex (Fig. 4D,E). tdTomato-positive neuronal processes were also observed throughout the utricle, saccule and cristae following tamoxifen delivery at E9.5 (Fig. 4G-I) indicating early expression in vestibular neurons as well. More importantly, tamoxifen induction at later stages (E11.5, E17.5) predominantly labels hair cells and not vestibular neurons demonstrating that, as in the SGNs, *Fgf8* expression is transient within vestibular neurons and restricted to early stages of neuronal development.

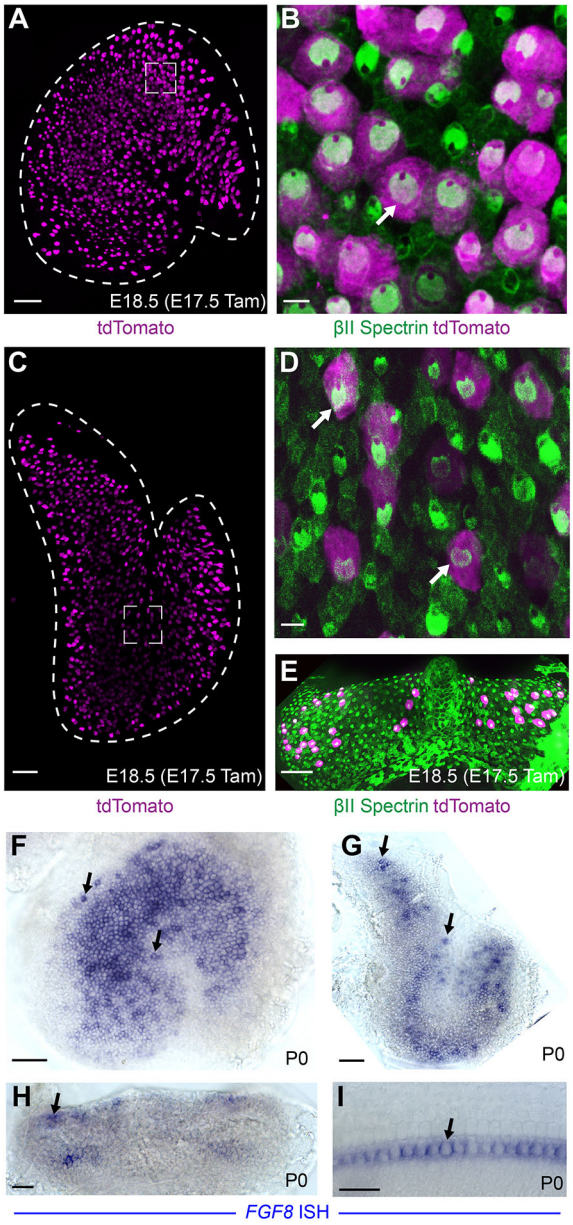

Fig. 2. *Fgf8*^{mcm} genetic labeling labels subsets of vestibular hair cells. (A) tdTomato fluorescence is present throughout the sensory epithelia in an *Fgf8*$^{mcm/+}$; ROSA$^{tdTom(Ai9)/WT}$ utricle at E18.5 following tamoxifen induction at E17.5. (B) Higher magnification image from the framed region in A shows tdTomato colocalization with βII spectrin (example marked by arrow). (C,E) tdTomato is also induced by *Fgf8*^{mcm} in vestibular hair cells throughout the saccule (C) and cristae (E). (D) Higher magnification image from the framed region in C shows tdTomato colocalization with βII spectrin (examples marked by arrows). (F-I) Whole-mount ISH for endogenous *Fgf8* in the utricle (F), saccule (G), cristae (H) and cochlea (I). Arrows highlight examples of mRNA expression in individual hair cells. Scale bars: 50 µm in A,C,E,F,G,H; 20 µm in B,D,I.

Development (2020) 147, dev192849. doi:10.1242/dev.192849

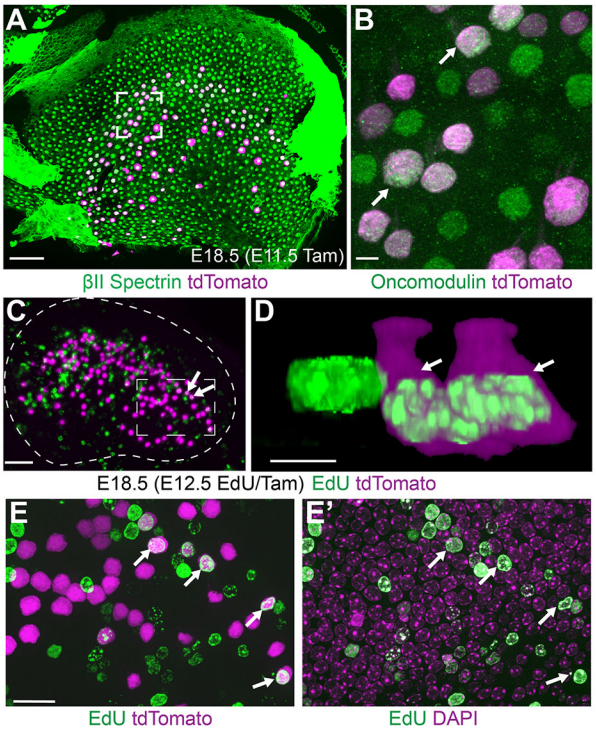

Fig. 3. *Fgf8*^{mcm} genetic labeling occurs shortly after hair cell terminal mitosis. (A) Tamoxifen induction at E11.5 induces tdTomato expression in hair cells throughout the central region of the utricle in which the striolar region lies at E18.5. (B) Higher magnification image from the framed region in A shows tdTomato colocalization with oncomodulin-positive hair cells (examples marked by arrows). (C) Newly divided hair cells labeled by EdU incorporation at E12.5 are genetically labeled by the tdTomato reporter with concurrent tamoxifen induction (examples marked by arrowheads). Dashed line indicates the boundary of the utricular sensory epithelium. (D) Higher magnification 3D-reconstruction of EdU-labeled hair cells. Arrowheads correspond to the two tdTomato-positive cells indicated in C. (E,E′) Higher magnification image corresponding to the framed region in C similarly reveals vestibular hair cells containing EdU and labeled by tdTomato (E) and DAPI (E′). Scale bars: 50 µm in A,C; 5 µm in B,D; 10 µm in E,E′.

Embryonic Fgf8^{mcm} genetic labeling selectively labels Type-I vestibular hair cells

The two different types of vestibular hair cells in the mouse can be distinguished from each other based upon morphologic and synaptic criteria which begin to emerge at about the time of birth (19 days post-copulation). These features were evaluated in cryosections collected from E18.5 *Fgf8*$^{mcm/+}$; tdTomato-positive embryos following tamoxifen induction at E17.5. At this early stage, many tdTomato-positive hair cells already exhibited an ampoule morphology characteristic of Type-I vestibular hair cells (Fig. 5A). Often, these putative Type-I hair cells were also contacted by a neuronal process that was immunoreactive for neurofilament (NFH) that appeared to be nascent calyceal termini, although formation of these synaptic structures is not complete until P14 (Fig. 5A′). Other tdTomato-positive hair cells had simpler or possibly immature synaptic contacts and hair cell morphologies that could not be distinguished from Type-II hair cells. Cells with these latter characteristics were more abundant in the periphery of the sensory epithelia.

A subset of Type-I hair cells produce oncomodulin, which is a calcium-binding protein found in Type-I hair cells populating the striolar region of the utricle, and are contacted by afferent neurons that form a complex calyx encompassing multiple hair cells. tdTomato and endogenous oncomodulin colocalize in the striolar region following tamoxifen induction at E17.5, consistent with *Fgf8* expression in Type-I hair cells (Fig. 5B). The striolar and extrastriolar regions also contain Type-I hair cells that are contacted by a simple calyx and do not express oncomodulin, but still develop the characteristic ampoule-like morphology of Type-I hair cells. 3D reconstruction of individual tdTomato-positive oncomodulin-negative cells from the striolar or medial and lateral extrastriolar regions revealed this stereotypic Type-I hair cell morphology (Fig. 5C-E). Altogether the morphology and overall distribution of genetically labeled cells is consistent with selective *Fgf8*^{mcm} activity in Type-I hair cells. tdTomato-positive cells with similar ampoule-like morphology were also seen in the saccule and semi-circular cristae, suggesting that *Fgf8* expression is a general marker of vestibular hair cell identity. The defining characteristic of Type-I hair cells is the calyceal synapse, which can be readily seen using neuronal markers such as βIII-tubulin at P14. To definitively establish whether embryonic hair cells expressing *Fgf8* differentiated into Type-I hair cells, tamoxifen was administered at E11.5 and tdTomato-positive hair cells were evaluated for the presence of a synaptic calyx at P14 (Fig. 6A). The majority of these cells were surrounded by a ring of βIII-tubulin, indicating the presence of a calyx and confirming Type-I hair cell identity.

Postnatal Fgf8 genetic labeling is restricted to Type-I hair cells

Recently it was proposed that hair cell sub-types differentiate sequentially, with the Type-II cells predominantly appearing at postnatal stages and, conversely, Type-I hair cells differentiating in the embryo (McInturff et al., 2018). In this scenario, genes expressed in hair cells at embryonic stages may appear to preferentially label Type-I hair cells in genetic labeling experiments, when in fact they may not be cell type-specific. To determine whether *Fgf8*^{mcm} sequentially labeled Type-I and then Type-II hair cells through the course of utricle development, tamoxifen was delivered at E11.5, E17.5, or P2. For each injection paradigm, tdTomato-positive cells were evaluated at P14 when cell type-specific molecular markers are available, such as the Type-I hair marker osteopontin, the Type-II markers Anxa4 and Calb2 (McInturff et al., 2018; Sayyid et al., 2019; Perry et al., 2003), or the presence of a calyx. Regardless of the time of tamoxifen induction, tdTomato genetic labeling predominantly labeled Type-I hair cells, as evidenced by the presence of calyceal synapses (Fig. 6A-C) and, at all stages, tamoxifen administration resulted in a comparable frequency of tdTomato-positive cells contacted by a calyx (Fig. 6D, Table S1).

The postnatal delivery of tamoxifen at P2 also failed to label cells expressing markers associated with Type-II hair cell identity. When evaluated at P14, very few tdTomato-positive hair cells expressed Type-II markers Anxa4 and Calb2 (Fig. 7B-D, Table S2). It is not unexpected that, on occasion, tdTomato was found in hair cells expressing Anxa4 or Calb2, as this marker is not absolutely restricted to Type-II hair cells and can be detected in a small proportion of cells expressing other Type-I markers (McInturff et al., 2018). In contrast, following tamoxifen delivery at P2, the majority of labeled hair cells colocalized with the Type-I marker osteopontin at P14 (Fig. 7A,D, Table S2). Finally, unlike the transient *Fgf8*^{mcm} activity observed in neurons, expression in hair cells appeared to be sustained across the range of developmental time points that tamoxifen was administered (E11.5 through P2).

Development (2020) 147, dev192849. doi:10.1242/dev.192849

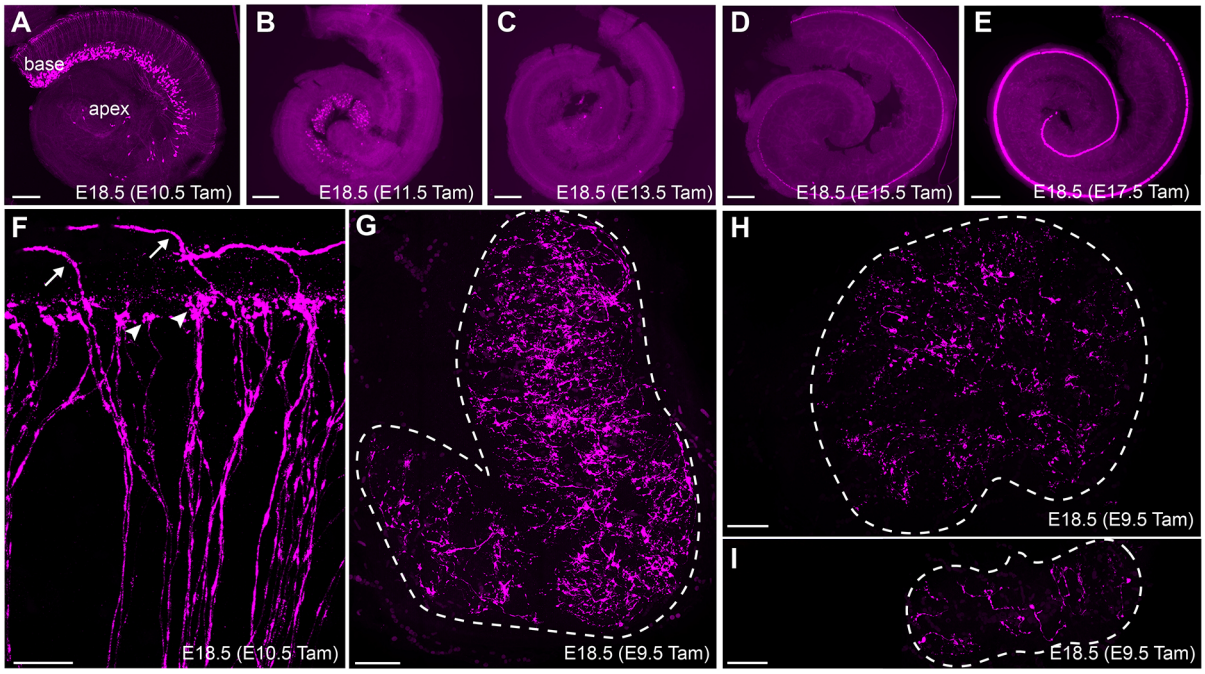

Fig. 4. *Fgf8* expression in auditory and vestibular neurons is transient. (A-E) *Fgf8*^{mcm} genetic labeling in the developing cochlea selectively labels SGNs following tamoxifen induction at E10.5 (A) and E11.5 (B). Little to no labeling is seen with tamoxifen induction at E13.5 (C), whereas inner hair cells are labeled following tamoxifen induction at E15.5 (D) and E17.5 (E). (F) Higher magnification image of tdTomato labeling in peripheral axons of auditory neurons following tamoxifen induction at E10.5 reveals Type-I SGNs (arrowheads) which innervate inner hair cells, and Type-II SGNs (arrows) that extend further, turn towards the cochlear base and innervate outer hair cells. (G-I) Tamoxifen induction at E9.5 labels the peripheral processes of vestibular neurons innervating the saccule (G), utricle (H) and cristae (I). Dashed line indicates the boundary of the vestibular sensory organ. Scale bars: 200 µm in A-E,G-I; 20 µm in F.

Hair cell development and innervation appears normal in Fgf8 CKOs

As FGFs are known secreted signaling molecules, restricted expression of *Fgf8* in Type-I hair cells suggests that FGF8 acts through autocrine and/or paracrine mechanisms during vestibule development. Consistent with a paracrine function in the cochlea, paracrine FGF8 signaling from inner hair cells promotes the differentiation of neighboring pillar cells (Jacques et al., 2007). Despite this, no phenotypic differences in hair cells or cellular organization within the vestibular maculae were identified in *Fgf8* CKOs compared with littermate controls (Fig. 8). CKOs were generated using two Cre lines frequently used for inner ear research, the hair cell-restricted *Atoh1*-Cre (Matei et al., 2005) and *Pax2*-Cre, which is active in the otic placode and also portions of the CNS and kidney (Ohyama and Groves, 2004). *Atoh1*-Cre-mediated gene deletion was incomplete as revealed by ISH, with some *Fgf8* mRNA persisting in the striolar region of the utricle at P0 (Fig. S2). *Pax2*-Cre on the other hand results in the complete loss of *Fgf8* mRNA throughout the utricle (Fig. S2); however, *Pax2*-Cre, *Fgf8* CKO mice die at birth. Based upon CKO phenotypes, *Fgf8* is not required for formation of the calyceal synapses that surround Type-I hair cells because these structures remain intact in extrastriolar regions of the utricle lacking *Fgf8* mRNA in *Atoh1*-Cre; *Fgf8* CKOs at P14 (Fig. 8A,B,I, Table S3). The number and distribution of Type-I hair cells as determined using oncomodulin to label Type-I hair cells in the striolar region (Fig. 8C,D,J, Table S3) and osteopontin to label Type-I hair cells in the extrastriolar regions (Fig. 8E,F,K) is also not changed in *Fgf8* CKOs. Finally, in the developing neocortex, Fgf8 acts in opposition to the transcription factor Emx2 to regulate cortical patterning (Fukuchi-Shimogori and Grove, 2003; Muzio and Mallamaci, 2003; O'Leary and Nakagawa, 2002; O'Leary and Sahara, 2008). Although Emx2 also functions in the utricle to regulate stereociliary bundle orientation and formation of the line of polarity reversal (Jiang et al., 2017), these features are not disrupted by the loss of *Fgf8* as there are no changes in hair cell polarity (Fig. 8G,H) or the relative position of the striolar region in *Pax2*-Cre; *Fgf8* CKOs (Fig. 8L).

DISCUSSION

Using CreER-mediated genetic labeling, we demonstrate temporally regulated, transient expression of *Fgf8* in auditory and vestibular neurons before E11.5 and sustained expression in Type-I vestibular hair cells at all subsequent developmental stages investigated (E11.5 to P2). We anticipate that the engineered *Fgf8*^{mcm} allele will be a valuable experimental resource that provides genetic access to this unique population of hair cells. This should enable further studies of vestibular development and regeneration, and create new approaches for understanding Type-I hair cell function through the application of genetically encoded tools for manipulating their function. *Fgf8*^{mcm} may also be applied for studies of cochlear inner hair cell function, in which selective *Fgf8* expression has been well documented (Jacques et al., 2007). The *Fgf8*^{mcm} allelic design also provides distinct advantages over alternative strategies for placing Cre recombinase at the *Fgf8* locus. First, insertion of the IRES:mER-Cre-mER expression cassette into the 3′UTR of *Fgf8* does not perturb its expression. This is significant because FGF8 signaling is dose dependent, as evidenced by severe developmental defects and lethality of hypomorphs (Frank et al., 2002; Meyers et al., 1998). Second, the tamoxifen-dependent CreER activity in the *Fgf8*^{mcm} line allows recombination to be restricted to hair cells and avoids recombination in those neurons that transiently express *Fgf8*. Finally, for developmental studies, the early onset of *Fgf8* expression, and hence CreER activity, will allow many target genes to be deleted before their transcription is initiated in hair cells.

Development (2020) 147, dev192849. doi:10.1242/dev.192849

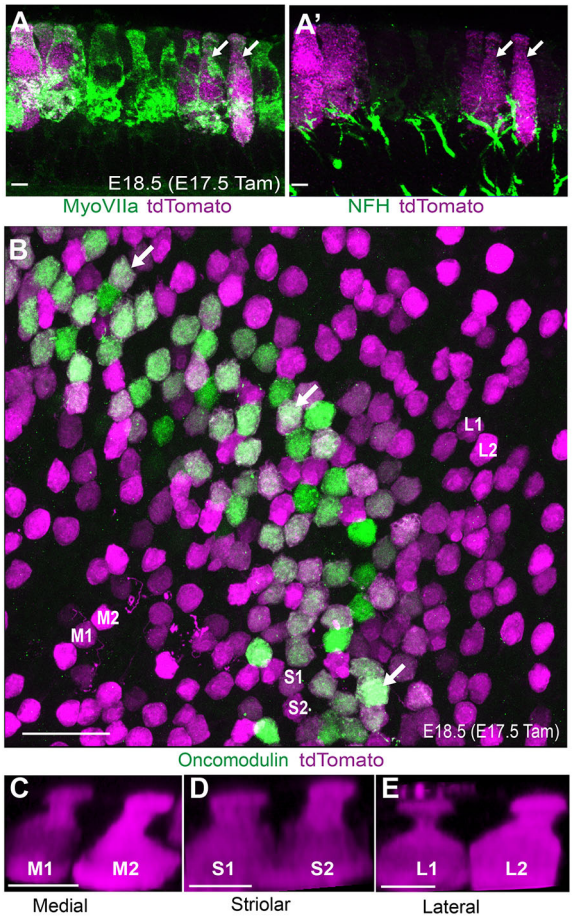

Fig. 5. *Fgf8*^{mcm} genetic labeling labels Type-I hair cells at embryonic stages. (A) Cross-section through the embryonic utricular sensory epithelia following tamoxifen induction at E17.5 showing tdTomato expression in hair cells with Type-I morphology characterized by a restriction at the apical neck (arrows). (A′) tdTomato-labeled hair cells are contacted by presumptive developing calyceal synapses (arrows). (B) Whole-mount immunolabeling of *Fgf8*^{mcm} utricle reveals colocation of tdTomato reporter and the striolar Type-I hair cell marker oncomodulin (examples illustrated by arrows). (C-E) 3D-reconstructions of tdTomato-positive oncomodulin-negative hair cells in medial extrastriolar (M1, M2; C), striolar (S1, S2; D), and lateral extrastriolar (L1, L2; E) regions also reveals ampoule-like Type-I hair cell morphology. Scale bars: 5 µm in A,C-E; 20 µm in B.

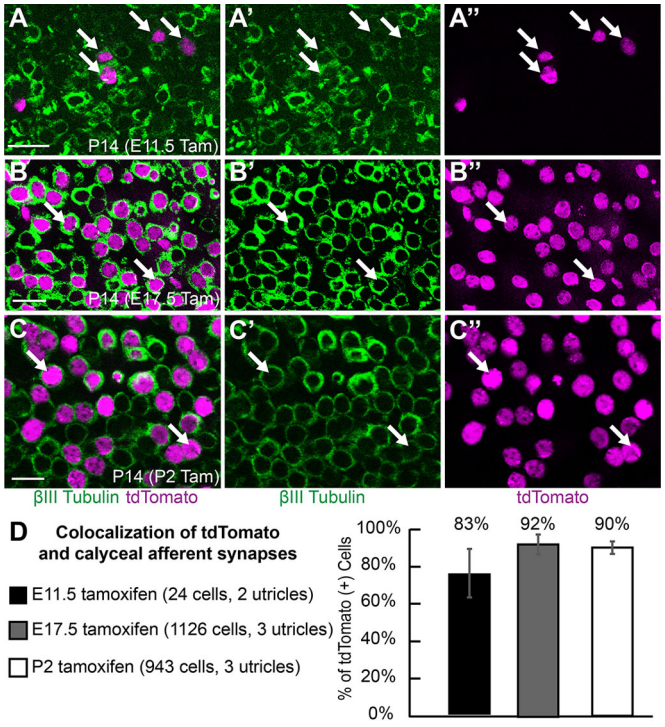

Fig. 6. *Fgf8*^{mcm} genetic labeling selectively labels Type-I hair cells contacted by calyxes. (A) Following tamoxifen induction at E11.5, tdTomato-positive hair cells are surrounded by βIII-tubulin rich calyces (arrows) when evaluated at P14, consistent with Type-I hair cell identity. (B) Following tamoxifen induction at E17.5, tdTomato-positive hair cells are surrounded by βIII-tubulin rich calyces (arrows) when evaluated at P14. (C) Following tamoxifen induction at P2, tdTomato-positive hair cells are similarly contacted by calyces (arrows) at P14. A′, B′, C′ show βIII-tubulin channel; A″, B″, C″ show tdTomato channel. (D) The frequency of calyx formation about tdTomato-positive hair cells following tamoxifen induction at different developmental stages. Data are mean±s.d. Scale bars: 10 µm.

Cre recombinase activity from the engineered *Fgf8*^{mcm} allele is detected in the utricular maculae at the earliest stages of hair cell differentiation, beginning shortly after terminal mitosis, and indicates that cell-type specification occurs earlier than has been documented using other criteria. Given the permanence of genetic labeling, it appears to be unlikely that *Fgf8* is expressed in Type-II hair cells or their precursors during this time. Consistent with this, tdTomato-positive hair cells at P14 express the Type-I marker osteopontin, rarely colocalize with the Type-II biased marker Anxa4, and are always contacted by calyceal synaptic endings. Perhaps more striking than this cell specificity is the observation that *Fgf8*^{mcm} can be activated in newly born hair cells at E11.5, a time when the initial cohort of hair cells is completing mitosis and beginning to differentiate. Together these observations suggest that vestibular hair cell identity is defined at the earliest stages of their development and refutes alternative models in which Type-I and Type-II hair cells are derived postnatally from a shared hair cell precursor.

It is more difficult to reconcile the early Type-I restricted expression of *Fgf8* with the potential role that Sox2 may have in defining vestibular hair cell identity after birth (Lu et al., 2019). The vestibular sensory epithelia are unique because expression of the progenitor cell marker *Sox2* is maintained throughout postnatal development in vestibular supporting cells and Type-II hair cells. Although *Sox2* is transiently expressed in Type-I hair cells, it is not downregulated until later stages, when these two cell types are readily distinguished using morphological and synaptic criteria. Based upon this correlation, *Sox2* downregulation after birth in a subset of cells has been suggested to be the mechanism by which the two hair cell types are established. Consistent with this potential mechanism, the postnatal deletion of *Sox2* results in an increase in the ratio of Type-I to Type-II hair cells (Lu et al., 2019). A parsimonious synthesis of the findings from these studies would be that *Fgf8* expression distinguishes between committed and non-committed states of cell fate divergence, and that only *Fgf8*-expressing cells are restricted to the Type-I identity. In contrast, *Fgf8*-negative cells may retain the potential to differentiate as either cell type, possibly doing so during postnatal development through a switching mechanism that is *Sox2*-dependent. It remains to be shown whether *Fgf8* expression is activated following *Sox2* gene deletion at postnatal stages or whether the two cohorts of Type-I hair cells that would be generated through these parallel paths might differ from each other.

Development (2020) 147, dev192849. doi:10.1242/dev.192849

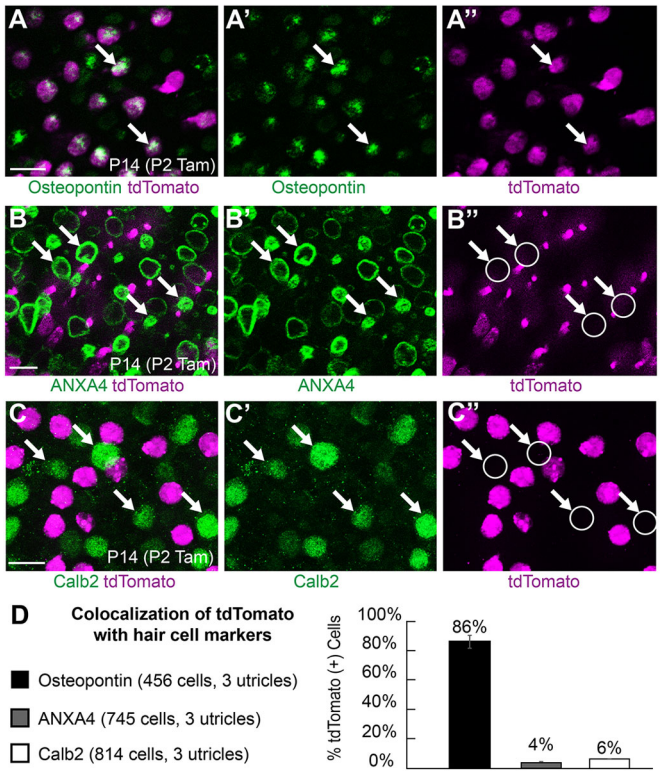

Fig. 7. *Fgf8*^{mcm} genetic labeling selectively labels Type-I but not Type-II hair cells at postnatal stages. (A-A″) tdTomato-positive hair cells labeled by tamoxifen induction at P2 colocalize with the Type-I hair cell marker osteopontin (examples marked by arrows). (B-B″) Hair cells labeled by tamoxifen induction at P2 (arrows) do not colocalize with the Type-II hair cell marker Anxa4. (C-C″) Hair cells labeled by tamoxifen induction at P2 do not colocalize with Type-II hair cell marker Calb2 (examples marked by arrows). (D) The frequency of tdTomato colocalization with cell type-specific markers following tamoxifen induction at P2. Data are mean±s.d. Scale bars: 10 µm.

Loss-of-function experiments using *Fgf8* CKOs generated with *Pax2*-Cre or *Atoh1*-Cre fail to demonstrate a requirement for FGF8 function during vestibular hair cell development. This is likely owing to genetic redundancy with other FGFs that preserve signaling in the absence of FGF8 and, consistent with this possibility, *Fgf3* and *Fgf10* are expressed during vestibular development in the mouse (Hossain and Morest, 2000; Pirvola et al., 2000; Ohuchi et al., 1997; Pauley et al., 2003). Furthermore, genetic redundancy in FGF signaling has been well described in cochlear development (Wright and Mansour, 2003; Mansour et al., 2013). One event where FGF8 functions independently is during pillar cell differentiation: the absence of *Fgf8* expression results in fewer pillar cells. FGF8 signals through FGFR3 to regulate pillar cell development in this context (Jacques et al., 2007). However, FGF8 must signal through different receptors in the utricle because FGFR3 is absent from the developing vestibule based upon genetic labeling experiments using *Fgfr3*-iCre mice (Fig. S3 and Anttonen et al., 2012). In contrast, *Fgfr1* and *Fgfr2* are expressed in vestibular hair cells of mice and rats, and these receptors are activated by FGF8 (Saffer et al., 1996; Burns et al., 2015; Pirvola et al., 2000). Moreover, the number of vestibular hair cells is reduced in *Fgfr1* CKO mice (Ono et al., 2014), and targeted deletion of *Fgfr2b* results in severe dysgenesis of the cochleovestibular labyrinth (Pirvola et al., 2000), demonstrating their necessity for vestibular morphogenesis and development. Together, these findings suggest that multiple FGFs are released by Type-I vestibular hair cells and may be received by FGFR1 and/or FGFR2 rather than FGFR3, as observed for FGF8-dependent pillar cell development in the cochlea.

As a secreted signaling molecule, FGF8 is most likely to function through a paracrine pathway to promote local differentiation or through an autologous mechanism that reinforces Type-I differentiation. Based upon FGF8 function in the cochlea, one role for FGF-signaling in vestibular sensory development may be to promote supporting cell differentiation. Unfortunately, the lack of molecular markers and evidence for supporting cell diversity in the utricle makes it difficult to test this hypothesis (Shim et al., 2005; Jacques et al., 2007). An exciting alternative is that FGF signaling directs afferent neuron differentiation and formation of the calyceal synapse that is unique to the Type-1 hair cells. The existence of a hair cell signal that directs post-synaptic specialization is suggested by the morphology of dimorphic afferent neurons, which contact both Type-I and Type-II hair cells but only form calyceal synaptic structures around the Type-I cell. Notably, FGF7 and FGF22 have been shown to promote the differentiation of excitatory and inhibitory synapses as presynaptic organizers (Terauchi et al., 2010), consistent with a potential role for FGF signaling in vestibular synaptic development. Finally, in the developing neocortex *Fgf8* regulates cortical patterning through a process called arealization, in which FGF8 expression in an anterior domain opposes the posterior expression of the transcription factor Emx2. We originally hypothesized that a similar process regulated *Emx2* expression in the utricle and thus determined the position of the line of polarity reversal that divides hair cells with opposite stereociliary bundle orientations (Deans, 2013; Jiang et al., 2017). However, the observed *Fgf8* expression throughout the utricle, including the Emx2-expressing domain in the lateral extrastriolar region, is inconsistent with this model. Moreover, the position of the line of polarity reversal is not altered in *Fgf8* mutants.

A remarkable characteristic of utricular hair cells in the mouse is their potential to regenerate at perinatal stages of development. Curiously, the majority of vestibular hair cells regenerated in the mouse are of the Type-II identity (Golub, 2012; Bucks, 2017). Understanding and directing this process to occur at later stages, and generating the correct proportion of hair cell types, is essential if regeneration strategies are to successfully replace lost hair cells. Although the contribution of FGF8 towards identity specification is not known, *Fgf8* expression in Type-I hair cells demonstrates that identity is established earlier than expected and shortly after terminal mitosis. This expression pattern further suggests that FGF or other morphogenic signaling pathways might be manipulated during the course of regeneration to direct cell fate. Thus, the *Fgf8*^{mcm} line may catalyze directed regeneration strategies, while the distinct cell-specific expression makes this line a valuable resource for studying hair cell development and function.

MATERIALS AND METHODS

Design and construction of the Fgf8^{mcm} allele

Fgf8^{mcm} mice were generated by inserting an IRES sequence (Jang and Wimmer, 1990; Kaminski et al., 1990) upstream of the *mER:Cre:mER* cDNA encoding a fusion protein with two copies of the mouse estrogen receptor (mER) flanking Cre recombinase, and a Neomycin-resistance (*NeoR*) selection cassette flanked by Frt recombination sites (Verrou et al., 1999). This assembly was inserted into an Eag1 site in the *Fgf8* gene located 36 bp 3′ of the *Fgf8* stop codon and 5′ to the endogenous polyadenylation sequence. The modified genomic fragment was shuttled into a plasmid backbone flanked by thymidine kinase genes. The linearized targeting vector was electroporated into mouse embryonic stem cells and subjected to selection with G418 and gancyclovir. Positive clones were identified by digesting

Development (2020) 147, dev192849. doi:10.1242/dev.192849

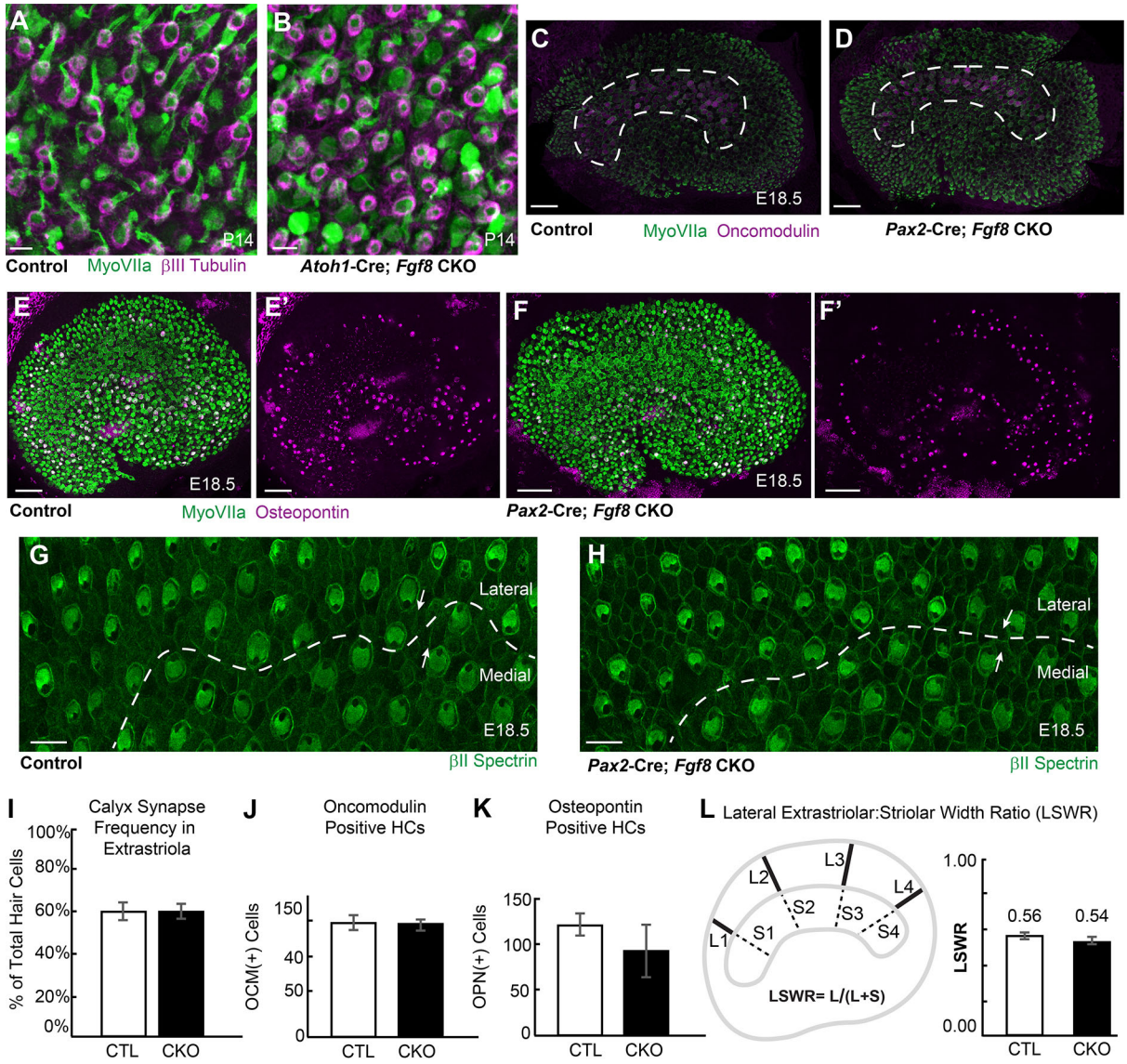

Fig. 8. *Fgf8* conditional knockout utricles are phenotypically normal. (A,B) Whole-mount immunolabeling using βIII-tubulin shows no changes in the average frequency of calyceal synapses in extrastriolar regions of *Atoh1*-Cre; *Fgf8* CKOs (B) and littermate control utricles (A) when evaluated at P14. (C,D) There are no differences in the distribution of oncomodulin-positive Type-I hair cells in the striolar region of *Pax2*-Cre; *Fgf8* CKO (D) compared with littermate control utricles (C) at E18.5. Dashed lines indicate the boundaries of the striolar region. (E-F′) There are no differences in the distribution of osteopontin-positive Type-I hair cells in the extrastriolar regions of *Pax2*-Cre*; Fgf8* CKO (F) compared with littermate control utricles (E) at E18.5. E′, F′ show osteopontin channel only. (G,H) A line of polarity reversal (dashed line) forms normally and stereociliary bundle orientation (arrows) is undisturbed in *Pax2*-Cre; *Fgf8* CKOs (H) similar to littermate controls (G). (I-K) The frequency of calyceal synapses (I) and number of Type-I hair cells expressing oncomodulin (J) and osteopontin (K) at E18.5 is not changed between littermate control (CTL) and *Fgf8* CKO utricles. (L) The position of the striolar region relative to the lateral border of the utricle is normal in the *Pax2*-Cre; *Fgf8* CKO utricle based upon measures of the lateral extrastriolar:striolar width ratio (LSWR). Data are mean±s.d. Scale bars: 10 µm in A,B,G,H; 50 µm C-F.

genomic DNA, Southern blotting, and hybridizing with a 3′ flanking probe, and targeted clones were confirmed to be correct by additional analyses using internal genomic probes and probes within the targeting vector. Following successful gene targeting the *NeoR* selection cassette was removed by Flp-mediated recombination of the flanking Frt sites. Genotyping of the wild-type and targeted alleles was performed by PCR using the following primers: *Fgf8* exon 5 sense 5′ GAGGTGCACTTCATGAAGCGC; *Fgf8* antisense, 5′ ATTTCAGGAGAACAGACCAGAG; sense for Frt site in mER:Cre:mER, 5′ ATACTATCTAGAGAATAGGAACTTCG.

Mouse strains and husbandry

For tamoxifen-inducible genetic labeling, $Fgf8^{mcm/+}$ males were crossed with $ROSA^{tdTom(Ai9)/tdTom(Ai9)}$ reporter mice (Madisen et al., 2010), and CreER was activated with a single intraperitoneal (IP) injection of tamoxifen (37.5-75 mg/kg, Sigma-Aldrich, #T5648) solubilized in corn oil and delivered to the timed-pregnant dam at embryonic stages ranging from E9.5 to E17.5 as indicated. When embryonic inductions were followed by postnatal collections, β-estradiol (75 µg/kg, Sigma-Aldrich, #E8875) was co-injected to help alleviate the anti-estrogen effects of tamoxifen. In some cases, where a natural birth did not occur on the 19th day of gestation, pups were delivered by Cesarean-section and cross fostered. Postnatal activation was carried out using a single IP injection of tamoxifen (75 mg/kg) at P2. For *Fgf8* mutant analysis, *Fgf8* CKOs were generated by crossing $Fgf8^{LoxP/LoxP}$ female mice with *Pax2*-Cre-positive or *Atoh1*-Cre-positive $Fgf8^{+/-}$ males. Cre-positive progeny were analyzed, with $Fgf8^{LoxP/-}$ mice serving as CKOs and $Fgf8^{LoxP/wt}$ as littermate controls. For these studies, *Pax2*-Cre mice (Ohyama and Groves, 2004) were provided by A. Groves (Baylor College of Medicine, Houston, TX, USA), *Atoh1*-Cre mice (Matei et al., 2005) and tdTom(Ai9) reporter mice were purchased from The Jackson Laboratory (Strains #011104 and #007909). *Fgf8* KO and $Fgf8^{Loxp/Loxp}$

Development (2020) 147, dev192849. doi:10.1242/dev.192849

lines have been previously described (Park et al., 2006). For timed breeding and tissue staging, noon on the day in which a vaginal plug was detected was considered E0.5 and the day of birth was considered P0. Mice of either sex were used interchangeably for all experimental analyses. Mouse colonies were maintained at the University of Utah under Institutional Animal Care and Use Committee approved guidelines, and genotyped using allele-specific PCR reactions.

Immunofluorescent labeling and imaging

Inner ear tissues were fixed using a 4% paraformaldehyde (PFA) solution prepared in 67 mM Sorensons' phosphate buffer (pH 7.4) for 2 h on ice. For whole-mount immunofluorescent labeling, inner ears were micro-dissected to isolate the cochlea or utricular maculae and detergent-permeabilized using blocking solution [5% normal donkey serum, 1% bovine serum albumin (BSA) in PBS] supplemented with 0.5% Triton X-100. Primary antibodies and Phalloidin Alexa Fluor 488 (Invitrogen, A12379, 1:1500) were diluted in blocking solution supplemented with 0.1% Tween-20 and incubated overnight at 4°C. For osteopontin and Anxa4 immunolabeling, tissue was fixed in 4% PFA prepared in PBS for 1 h at room temperature, and 10% donkey serum in PBS was used as a blocking solution as previously described (McInturff et al., 2018). Tissue was washed thoroughly using PBS with 0.05% Tween-20 and incubated with blocking solution supplemented with 0.1% Tween-20 and containing species-specific Alexa-conjugated secondary antibodies (Invitrogen: A11122, A21202, A31571; The Jackson Laboratory: 715-605-150, 705-165-147, 711-605-152; all diluted 1:1500). Tissue was washed thoroughly with PBS/0.05% Tween-20 and mounted for fluorescence microscopy using Prolong Gold Antifade Mountant (Thermo Fisher Scientific, #P10144). For immunolabeling of cryosections, tissue was fixed as described above using 4% PFA, cryoprotected by passing through a post-fixation sucrose gradient, and frozen in Neg50 (Richard Allan Scientific) before sectioning at 20 µm using a Leica CM3050 cryostat. Immunolabeling of tissue sections on SuperFrost Plus microscopy slides (Thermo Fisher Scientific, #12-550-15) was completed as described for whole-mount tissues except that Tween-20 was excluded from blocking and wash solutions. Fluorescent images were acquired using structured illumination microscopy using a Zeiss Axio Imager M.2 with ApoTome.2 attachment and an Axiocam 506 monochrome camera. Images were processed using Zeiss Zen software followed by figure preparation with Adobe Photoshop and Adobe Illustrator. 3D reconstructions of hair cells were completed using Fluorender software provided by University of Utah Scientific Computing and Imaging Institute. Quantification of hair cells or calyces, and area measurements, were facilitated by FIJI (ImageJ2). For measurements of the lateral extrastriolar:striolar width ratio the striolar region was defined by the presence of oncomodulin-positive hair cells and region boundaries were fit using the curvature tool (Adobe Illustrator) to demarcate the smallest area containing all of these cells. The boundaries of the utricular sensory epithelia were similarly demarcated based upon myosin VIIa labeling. Commercial antibodies used in this study were: goat anti-Anxa4 (R&D Systems, AF4146, 1:200), rabbit anti-βIII-tubulin (Covance, PRB-435P, 1:500), rabbit anti-dsRed to detect tdTomato (Clontech, 632496, 1:5000), mouse anti-myosin VIIa (Developmental Studies Hybridoma Bank, 138-1, deposited by D. J. Orten, 1:100), rabbit anti-myosin VIIa (Proteus Biosciences, 25-6790, 1:1000), rabbit anti-NF200 (Millipore, AB1989, 1:1500), goat anti-oncomodulin (Santa Cruz Biotechnology, sc-7466, 1:250), goat anti-osteopontin (R&D Systems, AF808, 1:200) and rat anti-tdTomato (Kerafast, EST203, 1:2000).

EdU birthdating

For EdU labeling of dividing cells, *Fgf8*$^{mcm/+}$ males were crossed with ROSA$^{tdTom(Ai9)/tdTom(Ai9)}$ reporter mice as previously described and pregnant dams received three IP injections of EdU (10 µg/kg) at 2 h apart on E12.5. Stock solutions of EdU (1 µg/µl) were prepared in PBS before injection and stored at −20°C. At E12.5, the pregnant dam was subsequently injected with 75 mg/kg tamoxifen to induce Cre-mediated genetic labeling as previously described. All embryos were collected at E18.5 and fixed in 4% PFA solution prepared in 67 mM Sorensons' phosphate buffer (pH 7.4) for 2 h on ice. Following dissection, tissue was permeabilized in PBS containing 0.5% Triton X-100 for 20 min, washed with three exchanges of PBS containing 3% BSA, and EdU was detected using the Click-iT cross-linking reaction and Alexa Fluor azide 488 dye as per the manufacturer's specifications (Thermo Fisher Scientific, C10337), with volumes adapted for a 96-well plate. Tissue was washed twice with two rapid exchanges of PBS containing 3% BSA and processed for whole-mount immunofluorescent labeling as previously described.

In situ hybridization

For whole-mount ISH, tissue was fixed using 4% PFA prepared in PBS (pH 7.4) overnight at 4°C and stored in 100% MeOH at −20°C. For whole-mount hybridization of inner ear tissues, ear capsules were dissected to expose sensory epithelia, which was subsequently rehydrated through a decreasing MeOH gradient [75%, 50%, 25% and then PBS with 0.05% Tween-20 (PBSt)]. Tissue was washed with PBSt, digested with 0.75 mg/ml Proteinase K (Ambion, #Am2546) for 25 min at room temperature, rinsed with PBSt, and subsequently fixed in 4% PFA/0.25% glutaraldehyde for 25 min at room temperature. Tissue was pre-hybridized for 3 h in 5× SSC hybridization buffer at 65°C and then hybridized with 150 ng/ml digoxigenin-labeled anti-sense probes for 18 h at 65°C with constant rocking. Tissue received three 50-min washes in 50% formamide, 2× SSC, 1% SDS solution, followed by 1 h in ISH blocking solution [1× MABT, 10% Blocking Reagent (Roche, #11-096-176-001), 2% and heat inactivated sheep serum]. Alkaline phosphatase-conjugated anti-digoxigenin antibodies (Roche, #11-093-274-910) were diluted 1:2500 in ISH blocking solution and rocked overnight at 4°C. After antibody labeling, tissue was washed six times for 1 h in Tris buffered saline with 0.05% Tween-20 (TBST) solution followed by alkaline phosphatase detection using BM Purple substrate (Roche, 11-442-074-001). After detection, tissues were post-fixed in 4% PFA/0.25% glutaraldehyde, cleared through an increasing MeOH gradient and mounted onto slides using Sorensons' phosphate buffer (pH 7.4), 31% glycerol, and 6.25% polyvinyl alcohol for imaging using the Zeiss Axio Imager M.2 and Axiocam 105 color camera. *Fgf8* mRNA distribution in wild-type mice and CKO mice was detected using an anti-sense *Fgf8* probe specific to *Fgf8* exon 5 which is deleted in CKOs, and was provided by S. Mansour (University of Utah).

Acknowledgements

We thank Suzanne Mansour and Lisa Urness for facilitating the exchange of mouse lines and ISH probe templates, and Orvelin Roman Jr and Sarah Siddoway for animal care and genotyping.

Competing interests

The authors declare no competing or financial interests.

Author contributions

Conceptualization: E.M.R., M.R.D.; Methodology: E.M.R.; Formal analysis: E.M.R.; Investigation: E.M.R., M.R.D.; Resources: A.M.M.; Writing - original draft: E.M.R.; Writing - review & editing: A.M.M., M.R.D.; Visualization: E.M.R.; Supervision: M.R.D.; Project administration: M.R.D.; Funding acquisition: M.R.D.

Funding

This work was supported by the National Institute on Deafness and Other Communication Disorders of the National Institutes of Health (NIH) (R01DC013066 to M.R.D.), and Eunice Kennedy Shriver National Institute of Child Health and Human Development of the NIH (T32HD007491 to E.M.R.). Deposited in PMC for release after 12 months.

Supplementary information

Supplementary information available online at
https://dev.biologists.org/lookup/doi/10.1242/dev.192849.supplemental

Peer review history

The peer review history is available online at
https://dev.biologists.org/lookup/doi/10.1242/dev.192849.reviewer-comments.pdf

References

Anttonen, T., Kirjavainen, A., Belevich, I., Laos, M., Richardson, W. D., Jokitalo, E., Brakebusch, C. and Pirvola, U. (2012). Cdc42-dependent structural development of auditory supporting cells is required for wound healing at adulthood. *Sci. Rep.* **2**, 978. doi:10.1038/srep00978

Boulet, A. M., Moon, A. M., Arenkiel, B. R. and Capecchi, M. R. (2004). The roles of Fgf4 and Fgf8 in limb bud initiation and outgrowth. *Dev. Biol.* **273**, 361-372. doi:10.1016/j.ydbio.2004.06.012

Burns, J. C., On, D., Baker, W., Collado, M. S. and Corwin, J. T. (2012). Over half the hair cells in the mouse utricle first appear after birth, with significant numbers originating from early postnatal mitotic production in peripheral and striolar growth zones. *J Assoc. Res. Otolaryngol.* **13**, 609-627. doi:10.1007/s10162-012-0337-0

Burns, J. C., Kelly, M. C., Hoa, M., Morell, R. J. and Kelley, M. W. (2015). Single-cell RNA-Seq resolves cellular complexity in sensory organs from the neonatal inner ear. *Nat. Commun.* **6**, 8557. doi:10.1038/ncomms9557

Bucks, S. A., Cox, B. C., Vlosich, B. A., Manning, J. P., Nguyen, T. B. and Stone, J. S. (2017). Supporting cells remove and replace sensory receptor hair cells in a balance organ of adult mice. *eLife* **6**, e18128. doi:10.7554/eLife.18128

Crespo-Enriquez, I., Partanen, J., Martinez, S. and Echevarria, D. (2012). Fgf8-related secondary organizers exert different polarizing planar instructions along the mouse anterior neural tube. *PLoS ONE* **7**, e39977. doi:10.1371/journal.pone.0039977

Crossley, P. H. and Martin, G. R. (1995). The mouse Fgf8 gene encodes a family of polypeptides and is expressed in regions that direct outgrowth and patterning in the developing embryo. *Development* **121**, 439-451.

Deans, M. R. (2013). A balance of form and function: planar polarity and development of the vestibular maculae. *Semin. Cell Dev. Biol.* **24**, 490-498. doi:10.1016/j.semcdb.2013.03.001

Eatock, R. A. and Songer, J. E. (2011). Vestibular hair cells and afferents: two channels for head motion signals. *Annu. Rev. Neurosci.* **34**, 501-534. doi:10.1146/annurev-neuro-061010-113710

Firnberg, N. and Neubüser, A. (2002). FGF signaling regulates expression of Tbx2, Erm, Pea3, and Pax3 in the early nasal region. *Dev. Biol.* **247**, 237-250. doi:10.1006/dbio.2002.0696

Frank, D. U., Fotheringham, L. K., Brewer, J. A., Muglia, L. J., Tristani-Firouzi, M., Capecchi, M. R. and Moon, A. M. (2002). An Fgf8 mouse mutant phenocopies human 22q11 deletion syndrome. *Development* **129**, 4591-4603.

Fukuchi-Shimogori, T. and Grove, E. A. (2001). Neocortex patterning by the secreted signaling molecule FGF8. *Science* **294**, 1071-1074. doi:10.1126/science.1064252

Fukuchi-Shimogori, T. and Grove, E. A. (2003). Emx2 patterns the neocortex by regulating FGF positional signaling. *Nat. Neurosci.* **6**, 825-831. doi:10.1038/nn1093

Gao, B., Ajima, R., Yang, W., Li, C., Song, H., Anderson, M. J., Liu, R. R., Lewandoski, M. B., Yamaguchi, T. P. and Yang, Y. (2018). Coordinated directional outgrowth and pattern formation by integration of Wnt5a and Fgf signaling in planar cell polarity. *Development* **145**, dev163824. doi:10.1242/dev.163824

Griffin, J. N., Compagnucci, C., Hu, D., Fish, J., Klein, O., Marcucio, R. and Depew, M. J. (2013). Fgf8 dosage determines midfacial integration and polarity within the nasal and optic capsules. *Dev. Biol.* **374**, 185-197. doi:10.1016/j.ydbio.2012.11.014

Golub, J. S., Tong, L., Ngyuen, T. B., Hume, C. R., Palmiter, R. D., Rubel, E. W. and Stone, J. S. (2012). Hair cell replacement in adult mouse utricles after targeted ablation of hair cells with diphtheria toxin. *J. Neurosci.* **32**, 15093-15105. doi:10.1523/JNEUROSCI.1709-12.2012

Hoffman, L. F., Choy, K. R., Sultemeier, D. R. and Simmons, D. D. (2018). Oncomodulin expression reveals new insights into the cellular organization of the murine utricle striola. *J. Assoc. Res. Otolaryngol.* **19**, 33-51. doi:10.1007/s10162-017-0652-6

Holley, M., Rhodes, C., Kneebone, A., Herde, M. K., Fleming, M. and Steel, K. P. (2010). Emx2 and early hair cell development in the mouse inner ear. *Dev. Biol.* **340**, 547-556. doi:10.1016/j.ydbio.2010.02.004

Hossain, W. A. and Morest, D. K. (2000). Fibroblast growth factors (FGF-1, FGF-2) promote migration and neurite growth of mouse cochlear ganglion cells in vitro: immunohistochemistry and antibody perturbation. *J. Neurosci. Res.* **62**, 40-55. doi:10.1002/1097-4547(20001001)62:1<40::AID-JNR5>3.0.CO;2-L

Hume, C. R., Bratt, D. L. and Oesterle, E. C. (2007). Expression of LHX3 and SOX2 during mouse inner ear development. *Gene Expr. Patterns* **7**, 798-807. doi:10.1016/j.modgep.2007.05.002

Jacques, B. E., Montcouquiol, M. E., Layman, E. M., Lewandoski, M. and Kelley, M. W. (2007). Fgf8 induces pillar cell fate and regulates cellular patterning in the mammalian cochlea. *Development* **134**, 3021-3029. doi:10.1242/dev.02874

Jang, S. K. and Wimmer, E. (1990). Cap-independent translation of encephalomyocarditis virus RNA: structural elements of the internal ribosomal entry site and involvement of a cellular 57-kD RNA-binding protein. *Genes Dev.* **4**, 1560-1572. doi:10.1101/gad.4.9.1560

Jiang, T., Kindt, K. and Wu, D. K. (2017). Transcription factor Emx2 controls stereociliary bundle orientation of sensory hair cells. *eLife* **6**, e23661. doi:10.7554/eLife.23661

Kaminski, A., Howell, M. T. and Jackson, R. J. (1990). Initiation of encephalomyocarditis virus RNA translation: the authentic initiation site is not selected by a scanning mechanism. *EMBO J.* **9**, 3753-3759. doi:10.1002/j.1460-2075.1990.tb07588.x

Koundakjian, E. J., Appler, J. L. and Goodrich, L. V. (2007). Auditory neurons make stereotyped wiring decisions before maturation of their targets. *J. Neurosci.* **27**, 14078-14088. doi:10.1523/JNEUROSCI.3765-07.2007

Lee, S. M., Danielian, P. S., Fritzsch, B. and Mcmahon, A. P. (1997). Evidence that FGF8 signalling from the midbrain-hindbrain junction regulates growth and polarity in the developing midbrain. *Development* **124**, 959-969.

Lewandoski, M., Sun, X. and Martin, G. R. (2000). Fgf8 signalling from the AER is essential for normal limb development. *Nat. Genet.* **26**, 460-463. doi:10.1038/82609

Lu, J., Hu, L., Ye, B., Hu, H., Tao, Y., Shu, Y., Chiang, H., Borse, V., Xiang, M., Wu, H. et al. (2019). Increased Type I and decreased Type II hair cells after deletion of Sox2 in the developing mouse utricle. *Neuroscience* **422**, 146-160. doi:10.1016/j.neuroscience.2019.09.027

Macatee, T. L., Hammond, B. P., Arenkiel, B. R., Francis, L., Frank, D. U. and Moon, A. M. (2003). Ablation of specific expression domains reveals discrete functions of ectoderm- and endoderm-derived FGF8 during cardiovascular and pharyngeal development. *Development* **130**, 6361-6374. doi:10.1242/dev.00850

Madisen, L., Zwingman, T. A., Sunkin, S. M., Oh, S. W., Zariwala, H. A., Gu, H., Ng, L. L., Palmiter, R. D., Hawrylycz, M. J., Jones, A. R. et al. (2010). A robust and high-throughput Cre reporting and characterization system for the whole mouse brain. *Nat. Neurosci.* **13**, 133-140. doi:10.1038/nn.2467

Mansour, S. L., Li, C. and Urness, L. D. (2013). Genetic rescue of Muenke syndrome model hearing loss reveals prolonged FGF-dependent plasticity in cochlear supporting cell fates. *Genes Dev.* **27**, 2320-2331. doi:10.1101/gad.228957.113

Matei, V., Pauley, S., Kaing, S., Rowitch, D., Beisel, K. W., Morris, K., Feng, F., Jones, K., Lee, J. and Fritzsch, B. (2005). Smaller inner ear sensory epithelia in Neurog1 null mice are related to earlier hair cell cycle exit. *Dev. Dyn.* **234**, 633-650. doi:10.1002/dvdy.20551

Mcinturff, S., Burns, J. C. and Kelley, M. W. (2018). Characterization of spatial and temporal development of type I and type II hair cells in the mouse utricle using new cell-type-specific markers. *Biol. Open* **7**, bio038083. doi:10.1242/bio.038083

Meyers, E. N., Lewandoski, M. and Martin, G. R. (1998). An Fgf8 mutant allelic series generated by Cre- and Flp-mediated recombination. *Nat. Genet.* **18**, 136-141. doi:10.1038/ng0298-136

Moon, A. M. and Capecchi, M. R. (2000). Fgf8 is required for outgrowth and patterning of the limbs. *Nat. Genet.* **26**, 455-459. doi:10.1038/82601

Muzio, L. and Mallamaci, A. (2003). Emx1, emx2 and pax6 in specification, regionalization and arealization of the cerebral cortex. *Cereb. Cortex.* **13**, 641-647. doi:10.1093/cercor/13.6.641

Oesterle, E. C., Campbell, S., Taylor, R. R., Forge, A. and Hume, C. R. (2008). Sox2 and JAGGED1 expression in normal and drug-damaged adult mouse inner ear. *J. Assoc. Res. Otolaryngol.* **9**, 65-89. doi:10.1007/s10162-007-0106-7

Ohuchi, H., Nakagawa, T., Yamamoto, A., Araga, A., Ohata, T., Ishimaru, Y., Yoshioka, H., Kuwana, T., Nohno, T., Yamasaki, M. et al. (1997). The mesenchymal factor, FGF10, initiates and maintains the outgrowth of the chick limb bud through interaction with FGF8, an apical ectodermal factor. *Development* **124**, 2235-2244.

Ohyama, T. and Groves, A. K. (2004). Generation of Pax2-Cre mice by modification of a Pax2 bacterial artificial chromosome. *Genesis* **38**, 195-199. doi:10.1002/gene.20017

O'Leary, D. D. M. and Nakagawa, Y. (2002). Patterning centers, regulatory genes and extrinsic mechanisms controlling arealization of the neocortex. *Curr. Opin. Neurobiol.* **12**, 14-25. doi:10.1016/S0959-4388(02)00285-4

O'Leary, D. D. M. and Sahara, S. (2008). Genetic regulation of arealization of the neocortex. *Curr. Opin. Neurobiol.* **18**, 90-100. doi:10.1016/j.conb.2008.05.011

Ono, K., Kita, T., Sato, S., O'Neill, P., Mak, S.-S., Paschaki, M., Ito, M., Gotoh, N., Kawakami, K., Sasai, Y. et al. (2014). FGFR1-Frs2/3 signalling maintains sensory progenitors during inner ear hair cell formation. *PLoS Genet.* **10**, e1004118. doi:10.1371/journal.pgen.1004118

Ornitz, D. M., Xu, J., Colvin, J. S., Mcewen, D. G., Macarthur, C. A., Coulier, F., Gao, G. and Goldfarb, M. (1996). Receptor specificity of the fibroblast growth factor family. *J. Biol. Chem.* **271**, 15292-15297. doi:10.1074/jbc.271.25.15292

Park, E. J., Ogden, L. A., Talbot, A., Evans, S., Cai, C.-L., Black, B. L., Frank, D. U. and Moon, A. M. (2006). Required, tissue-specific roles for Fgf8 in outflow tract formation and remodeling. *Development* **133**, 2419-2433. doi:10.1242/dev.02367

Pauley, S., Wright, T. J., Pirvola, U., Ornitz, D., Beisel, K. and Fritzsch, B. (2003). Expression and function of FGF10 in mammalian inner ear development. *Dev. Dyn.* **227**, 203-215. doi:10.1002/dvdy.10297

Perry, B., Jensen-Smith, H. C., Ludueña, R. F. and Hallworth, R. (2003). Selective expression of β tubulin isotypes in gerbil vestibular sensory epithelia and neurons. *J. Assoc. Res. Otolaryngol.* **4**, 329-338. doi:10.1007/s10162-002-2048-4

Pirvola, U., Spencer-Dene, B., Xing-Qun, L., Kettunen, P., Thesleff, I., Fritzsch, B., Dickson, C. and Ylikoski, J. (2000). FGF/FGFR-2(IIIb) signaling is essential for inner ear morphogenesis. *J. Neurosci.* **20**, 6125-6134. doi:10.1523/JNEUROSCI.20-16-06125.2000

Raft, S., Koundakjian, E. J., Quinones, H., Jayasena, C. S., Goodrich, L. V., Johnson, J. E., Segil, N. and Groves, A. K. (2007). Cross-regulation of Ngn1 and Math1 coordinates the production of neurons and sensory hair cells during inner ear development. *Development* **134**, 4405-4415. doi:10.1242/dev.009118

Reifers, F., Bohli, H., Walsh, E. C., Crossley, P. H., Stainier, D. Y. and Brand, M. (1998). Fgf8 is mutated in zebrafish acerebellar (ace) mutants and is required for maintenance of midbrain-hindbrain boundary development and somitogenesis. *Development* **125**, 2381-2395.

Rennie, K. J., Ricci, A. J. and Correia, M. J. (1996). Electrical filtering in gerbil isolated type I semicircular canal hair cells. *J. Neurophysiol.* **75**, 2117-2123. doi:10.1152/jn.1996.75.5.2117

Roehl, H. and Nüsslein-Volhard, C. (2001). Zebrafish pea3 and erm are general targets of FGF8 signaling. *Curr. Biol.* **11**, 503-507. doi:10.1016/S0960-9822(01)00143-9

Ruben, R. J. (1967). Development of the inner ear of the mouse: a radioautographic study of terminal mitoses. *Acta Otolaryngol.* **220** Suppl., 1-44.

Rüsch, A., Lysakowski, A. and Eatock, R. A. (1998). Postnatal development of type I and type II hair cells in the mouse utricle: acquisition of voltage-gated conductances and differentiated morphology. *J. Neurosci.* **18**, 7487-7501. doi:10.1523/JNEUROSCI.18-18-07487.1998

Saffer, L. D., Gu, R. and Corwin, J. T. (1996). An RT-PCR analysis of mRNA for growth factor receptors in damaged and control sensory epithelia of rat utricles. *Hear. Res.* **94**, 14-23. doi:10.1016/0378-5955(95)00228-6

Sayyid, Z. N., Wang, T., Chen, L., Jones, S. M. and Cheng, A. G. (2019). Atoh1 directs regeneration and functional recovery of the mature mouse vestibular system. *Cell Rep.* **28**, 312-324.e4. doi:10.1016/j.celrep.2019.06.028

Shim, K., Minowada, G., Coling, D. E. and Martin, G. R. (2005). Sprouty2, a mouse deafness gene, regulates cell fate decisions in the auditory sensory epithelium by antagonizing FGF signaling. *Dev. Cell* **8**, 553-564. doi:10.1016/j.devcel.2005.02.009

Simmons, D. D., Tong, B., Schrader, A. D. and Hornak, A. J. (2010). Oncomodulin identifies different hair cell types in the mammalian inner ear. *J. Comp. Neurol.* **518**, 3785-3802. doi:10.1002/cne.22424

Sun, X., Meyers, E. N., Lewandoski, M. and Martin, G. R. (1999). Targeted disruption of Fgf8 causes failure of cell migration in the gastrulating mouse embryo. *Genes Dev.* **13**, 1834-1846. doi:10.1101/gad.13.14.1834

Terauchi, A., Johnson-Venkatesh, E. M., Toth, A. B., Javed, D., Sutton, M. A. and Umemori, H. (2010). Distinct FGFs promote differentiation of excitatory and inhibitory synapses. *Nature* **465**, 783-787. doi:10.1038/nature09041

Verrou, C., Zhang, Y., Zürn, C., Schamel, W. W. A. and Reth, M. (1999). Comparison of the tamoxifen regulated chimeric Cre recombinases MerCreMer and CreMer. *Biol. Chem.* **380**, 1435-1438. doi:10.1515/BC.1999.184

Warchol, M. E., Massoodnia, R., Pujol, R., Cox, B. C. and Stone, J. S. (2019). Development of hair cell phenotype and calyx nerve terminals in the neonatal mouse utricle. *J. Comp. Neurol.* **527**, 1913-1928. doi:10.1002/cne.24658

Wright, T. J. and Mansour, S. L. (2003). Fgf3 and Fgf10 are required for mouse otic placode induction. *Development* **130**, 3379-3390. doi:10.1242/dev.00555

Zhang, Y., Riesterer, C., Ayrall, A.-M., Sablitzky, F., Littlewood, T. D. and Reth, M. (1996). Inducible site-directed recombination in mouse embryonic stem cells. *Nucleic Acids Res.* **24**, 543-548. doi:10.1093/nar/24.4.543

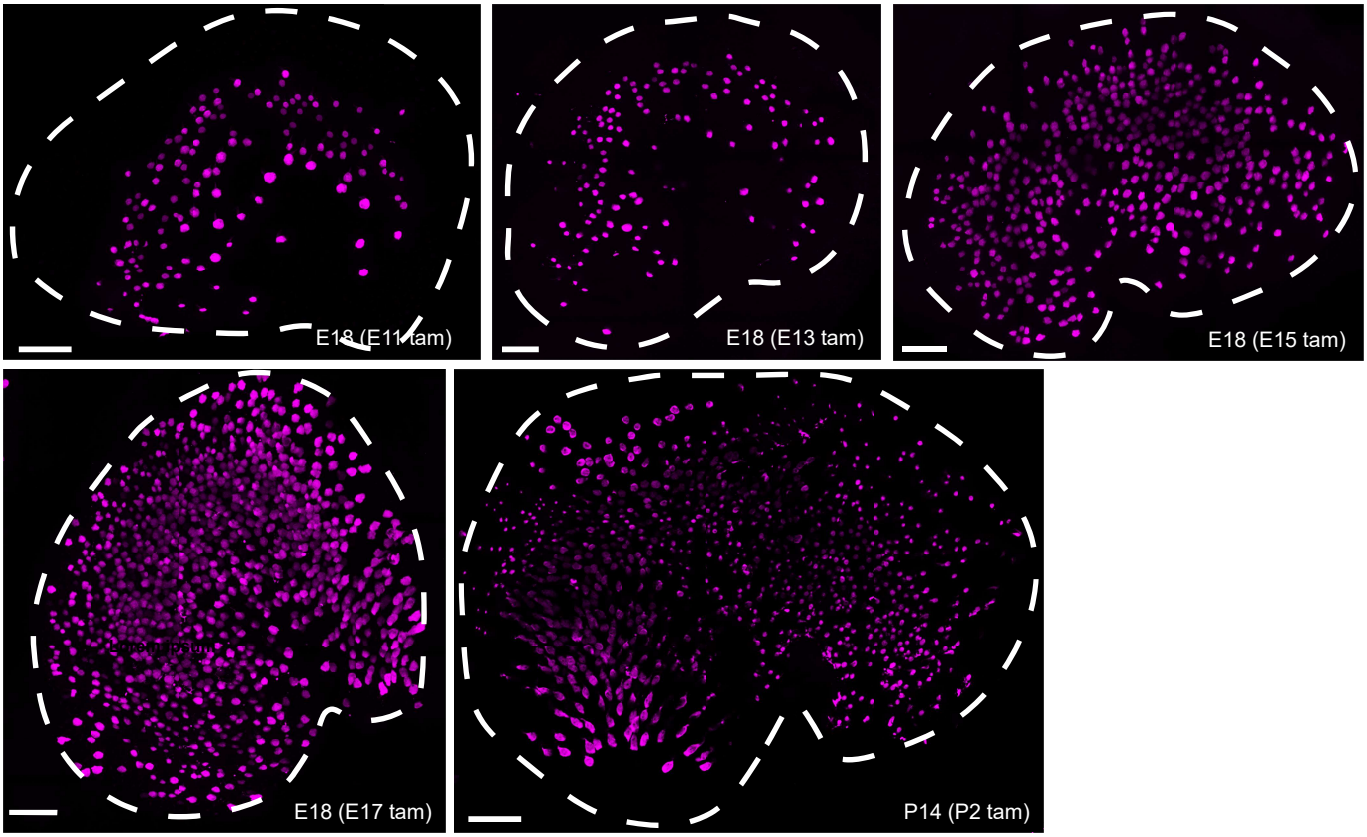

Figure S1. Timecourse of Fgf8 ^{mcm} genetic labeling in the developing mouse utricle. tdTomato labeling of utricular hair cells following a single dose of tamoxifen delivered at **(A)** E11.5, **(B)** E13.5, **(C)** E15.5 or **(D)** E17.5 and evaluated at E18.5. **(E)** tdTomato labeling of utricular hair cells following a single dose of tamoxifen delivered at P2 and evaluated at P14. Panels (A) and (D) are reprinted from primary figures. Scale bars: (50 μm)

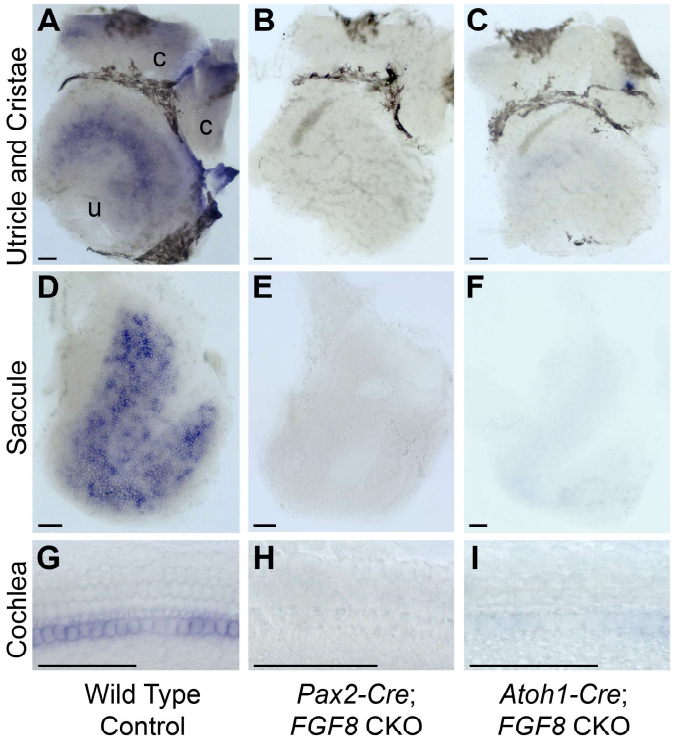

Figure S2. Fgf8 expression is abolished in *Pax2*-Cre and *Atoh1*-Cre; *Fgf8* CKOs
(A) Wholemount ISH for *Fgf8* shows vestibular hair cell expression in littermate control utricle (u) and cristae (c), saccule (D), and inner hair cells (G) of the organ of Corti. (B,E,H) *Fgf8* mRNA is completely lost following gene deletion using *Pax2*-Cre in each of these sensory epithelia. (C,F) *Fgf8* mRNA is lost from the extrastriolar regions of the utricle and saccule and the inner hair cells (I) of the organ of Corti following hair cell specific deletion using *Atoh1*-Cre. Brackets indicate the he approximate boundaries of the striolar region. Scale bars: (50μm)

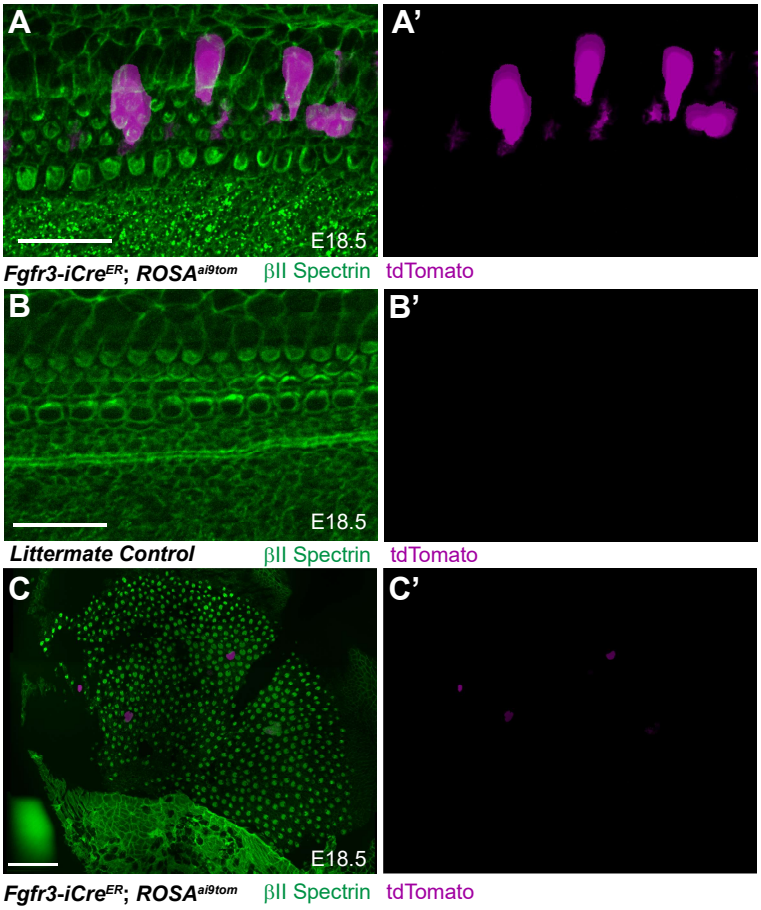

Figure S3. Fgfr3 expression is absent from the majority of the utricle
(A) Fgfr3-iCreER tdTomato labeling of cells in the organ of Corti following daily tamoxifen injections from E9.5 to E12.5. **(B)** Cre negative littermate control cochlea showing activation of the tdTomato reporter. **(C)** Fgfr3-iCreER shows minimal labeling of the utricle following the same tamoxifen regimen. βII-spectrin labeling shows the distribution of vestibular hair cells.
Scale bars: 20μm (A,B); 50μm (C).

P14 (E11.5 Tam) from Fig. 6D

Utricle	tdTomato (+)	tdTomato(+) w/ Calyx	% Colocalized	Mean	83%
1	12	9	75%	STDEV	12%
2	12	11	92%	STDERROR	8%
				√N	1.4

P14 (E17.5 Tam) from Fig. 6D

Utricle	tdTomato (+)	tdTomato(+) w/ Calyx	% Colocalized	Mean	92%
1	360	354	98%	STDEV	6%
2	300	277	92%	STDERROR	3%
3	466	403	86%	√N	1.7

P14 (P2 Tam) from Fig. 6D

Utricle	tdTomato (+)	tdTomato(+) w/ Calyx	% Colocalized	Mean	90%
1	34	33	97%	STDEV	7%
2	445	374	84%	STDERROR	4%
3	464	419	90%	√N	1.7

Table S1. Raw data used for quantification graphs presented in Figure 6

P14 (P2 Tam) from Fig. 7D

Utricle	tdTomato (+)	tdTomato (+) w/ OPN	% Colocalized	Mean	86%
1	205	188	92%	STDEV	9%
2	206	187	91%	STDERROR	5%
3	45	34	76%	√N	1.7

P14 (P2 Tam) from Fig. 7D

Utricle	tdTomato (+)	tdTomato (+) w/ Calb2	% Colocalized	Mean	6%
1	28	1	4%	STDEV	5%
2	390	46	12%	STDERROR	3%
3	396	12	3%	√N	1.7

P14 (P2 Tam) from Fig. 7D

Utricle	tdTomato (+)	tdTomato (+) w/ Anxa4	% Colocalized	Mean	4%
1	149	9	6%	STDEV	2%
2	321	10	3%	STDERROR	1%
3	275	10	4%	√N	1.7

Table S2. Raw data used for quantification graphs presented in Figure 7

P14 from Fig. 8I

Utricle	Genotype	MyoVIIa	BIII Tubulin+MyoVIIa	% HCs with Calyx	Mean	61%
1	Littermate Control	778	511	66%	STDEV	4%
2	Littermate Control	845	486	58%	STDERROR	2%
3	Littermate Control	945	566	60%	√N	1.7

Utricle	Genotype	MyoVIIa	BIII Tubulin+MyoVIIa	% HCs with Calyx	Mean	61%
1	*Atoh1-Cre*;*Fgf8* CKO	955	525	55%	STDEV	5%
2	*Atoh1-Cre*;*Fgf8* CKO	914	575	63%	STDERROR	3%
3	*Atoh1-Cre*;*Fgf8* CKO	913	590	65%	√N	1.7

P14 from Fig. 8J

Utricle	Genotype	OPN	Mean	121
1	Littermate Control	138	STDEV	20
2	Littermate Control	99	STDERROR	12
3	Littermate Control	127	√N	1.73

Utricle	Genotype	OPN	Mean	93
1	*Pax2-Cre*; *Fgf8* CKO	149	STDEV	51
2	*Pax2-Cre*; *Fgf8* CKO	50	STDERROR	29
3	*Pax2-Cre*; *Fgf8* CKO	79	√N	1.73

P14 from Fig. 8J

Utricle	Genotype	OCM	Mean	123
1	Littermate Control	134	STDEV	17
2	Littermate Control	104	STDERROR	8
3	Littermate Control	140	√N	2.00
4	Littermate Control	114		

Utricle	Genotype	OCM	Mean	122
1	*Pax2-Cre*; *Fgf8* CKO	128	STDEV	10
2	*Pax2-Cre*; *Fgf8* CKO	110	STDERROR	6
3	*Pax2-Cre*; *Fgf8* CKO	128	√N	1.73

P14 from Fig. 8J

Utricle	Genotype	Mean LWSR	Mean	0.56
1	Littermate Control	0.51	STDEV	0.04
2	Littermate Control	0.57	STDERROR	0.02
3	Littermate Control	0.56	√N	2.45
4	Littermate Control	0.55		
5	Littermate Control	0.55		
6	Littermate Control	0.56		
7	Littermate Control	0.55		
8	Littermate Control	0.66		

Utricle	Genotype	Mean LWSR	Mean	0.54
1	*Pax2-Cre*; *Fgf8* CKO	0.56	STDEV	0.08
2	*Pax2-Cre*; *Fgf8* CKO	0.45	STDERROR	0.03
3	*Pax2-Cre*; *Fgf8* CKO	0.51	√N	2.45
4	*Pax2-Cre*; *Fgf8* CKO	0.70		
5	*Pax2-Cre*; *Fgf8* CKO	0.56		
6	*Pax2-Cre*; *Fgf8* CKO	0.49		
7	*Pax2-Cre*; *Fgf8* CKO	0.47		

Table S3. Raw data used for quantification graphs presented in Figure 8
Comparison of E18.5 Pax2-Cre; Fgf8 CKO utricles to littermate controls for presence of Type I hair cells in the striola Oncomodulin and extrastriola with Osteopontin from Fig. 8J and Lateral extrastriolar width to striolar width ratio (LWSR) compared between E18.5 Pax2-Cre; Fgf8 CKO utricles corresponding to Fig. 8J.